Journal of Applied Fluid Mechanics, Vol. 9, No. 4, pp. 1753-1762, 2016.
Available online at www.jafmonline.net, ISSN 1735-3572, EISSN 1735-3645.
DOI: 10.18869/acadpub.jafm.68.235.24323

Mixed Convection Falkner-Skan Wedge Flow of an Oldroyd-B Fluid in Presence of Thermal Radiation

M. Bilal Ashraf [1†], T. Hayat[2,3], and H. Alsulami[3]

[1] Department of Mathematics, Comsats Institute of Information Technology WahCantt. 47040, Pakistan
[2] Department of Mathematics, Quaid-i-Azam University 45320 Islamabad 44000, Pakistan
[3] Department of Mathematics, Faculty of Science, King Abdulaziz University, P. O. Box 80203, Jeddah 21589, Saudi Arabia

†Corresponding Author Email: bilalashraf_qau@yahoo.com

(Received December 11, 2014; accepted February 9, 2015)

ABSTRACT

The present study deals with the Falkner-Skan flow of rate type non-Newtonian fluid. Expressions of an Oldroyd-B fluid in the presence of mixed convection and thermal radiation are used in the development of relevant equations. The resulting partial differential equations are reduced into the ordinary differential equations employing appropriate transformations. Expressions of flow and heat transfer are constructed. Convergence of derived nonsimilar series solutions is guaranteed. Impact of various parameters involved in the flow and heat transfer results is plotted and examined.

Keywords: Oldroyd-B fluid; Mixed convection; Thermal radiation; Falkner-Skan flow.

NOMENCLATURE

c_p	specific heat
g	gravitational acceleration
Gr_x	the local Grashof number
k_T	thermal conductivity
Nu	local Nusselt number
Pr	Prandtl number
R	radiation parameter
Re_x	is the local Reynold number
u and v	are velocity components
μ	is dynamic viscosity
ρ	density of fluid
α	wedge angle
λ_1	is the relaxation time,
λ_2	is the retardation time,
λ	mixed convection parameter
β_1 and β_2	are the dimensionless parameters

1. INTRODUCTION

The non-Newtonian fluids are encountered in the industrial and technological applications. Many fluids in nature do not obey the Newton's law of viscosity. Such fluids include polymer solutions, colloidal and suspension solutions, apple sauce, clay coating, shampoos, paints, certain oils, cement, sludge, drilling muds, food products, paper pulp, aqueous foams, slurries, grease etc. The rheological characteristics of non-Newtonian fluids cannot be predicted by employing a single relationship between stress and shear rate. Hence the non-Newtonian fluids are mainly classified into three types namely, the integral, differential and rate. Extensive studies in the literature have been devoted to the flows of differential type fluids in various geometries. However the differential type fluids are insufficient to describe the effects of relaxation and retardation times although they own the properties of normal stress, shear thinning and shear thickening. The rate type fluids are significant for the description of relaxation and retardation times effects. Oldroyd-B model is known as one of the subclass of rate type models which can predict the effects of relaxation and retardation times. Some of the recent studies relevant to Oldroyd-B model include the researches of (Fetecau *et al*. 2010, Fetecau *et al*. 2009, Zheng *et al*. 2011, Haitao *et al*. 2009a, Haitao *et al*. 2009b, Liu *et al*. 2011, Zheng *et al*. 2011, Fetecau *et al*. 2011, Jamil *et al*. 2011, Hayat *et al*. 2012).

In the field of aerodynamics, the analysis of two-dimensional boundary layer problems for steady and incompressible flow passing a wedge is common area of interest. The study of heat transfer along a wedge has gained considerable attention due to its vast applications in industry and its important bearings in several technological and natural processes. Falkner and Skan (1931) firstly discussed the momentum boundary layer equation of two-dimensional wedge flows. They proposed a similarity transformation method in order to reduce the partial differential equation to the non-linear third order ordinary differential equation. Afterwards Hartee (1937) found the solution of that problem and also obtained the numerical values of the wall shear stress for different values of wedge angle. Abbasbandy and Hayat (2009) employed Hankel-Pade method to calculate the skin friction coefficients of the MHD Falkner-Skan boundary layer flow of viscous fluid. In another article, Abbasbandy and Hayat (2009) used the homotopy analysis method to obtain the analytic solution to this problem. Prand *et al*. (2011) established the MHD Falkner-Skan flow on a fixed and impermeable wedge by using the pseudospectral method of the Hermite functions. Kuo (2005) employed the differential transform method to analyze the heat transfer in the Falkner-Skan wedge flow. Radiative effects have important applications in several problems of physics and engineering. The radiation heat transfer effects in different flows are important in space technology and high temperature process. But a very little is known about the effects of radiation in the boundary layer flow of rate type fluids. Thermal radiation effects may play an important role in controlling heat transfer in polymer processing industry where the quality of the final product depends on the heat controlling factors to some extent. High temperature plasmas, cooling of nuclear reactors, liquid metal fluids, power generation systems are some important applications of radiative heat transfer from a wall to conductive gray fluids. A very significant area of research in radiative heat transfer, at the present time is the numerical simulation of combined radiation and convection / conduction transport processes. The effort has arisen largely due to the need to optimize industrial system such as furnaces, ovens and boilers and the interest in our environment and in no conventional energy sources, such as the use of salt gradient solar ponds for energy collection and storage. In particular, mixed convection induced by the simultaneous action of buoyancy forces resulting from thermal diffusion is of considerable interest in nature and in many industrial applications such as geophysics, oceanography, drying processes, solidification of binary alloy and chemical engineering. The effect of radiation in heat transfer problems have been studied by Chen (2009), Mukhopadhyay (2009) and Hayat *et al*. (2010). Recently, Kim (2001) developed the numerical treatment for the Falkner-Skan wedge flow of a power law fluid. Hayat *et al*. (2011) extended the analysis of Kim (2001) for mixed convection. Ishak (2010) presented the similar solutions for flow and heat transfer over a permeable surface with convective boundary conditions.

The aim of present paper is to analyze the radiative Falkner-Skan flow of an Oldroyd-B fluid in the presence of mixed convection. The presentation of article is made as follows. Problem is formulated in the next section. Section three consists of the series solutions of the governing problem by using a very useful technique namely the homotopy analysis method (Liao (2012), Liu (2013), Hayat *et al*. (2013), Abbasbandy *et al*. (2013), Zheng *et al*. (2012), Rashidi *et al*. (2014), Turkyilmazoglu (2012), Ashraf *et al*. (2015)). Convergence analysis and the impact of various parameters of interest are presented in section four. The last section includes the main observations.

2. PROBLEM DEVELOPMENT

Let us investigate the two-dimensional Falkner-Skan flow of an Oldroyd-B fluid. We further consider the heat transfer. Cartesian coordinates (x, y) are used such that x -axis is parallel to the wall and y -axis normal to it. An incompressible fluid occupies the region $y \geq 0$. The equations governing the present flow situation are based on the conservation laws of mass, linear momentum and energy. Flow diagram of the problem is as follows:

Taking into account the aforementioned assumptions, the resulting boundary layer equations can be written as follows:

$$\frac{\partial u}{\partial x}+\frac{\partial v}{\partial y}=0, \tag{1}$$

$$\begin{aligned} u\frac{\partial u}{\partial x}+v\frac{\partial u}{\partial y} &= \nu\frac{\partial^2 u}{\partial y^2} \\ &-\lambda_1\left[u^2\frac{\partial^2 u}{\partial x^2}+v^2\frac{\partial^2 u}{\partial y^2}+2uv\frac{\partial^2 u}{\partial x\,\partial y}\right] \\ &+\nu\lambda_2\left[u\frac{\partial^3 u}{\partial x\,\partial y^2}+v\frac{\partial^3 u}{\partial y^3}-\frac{\partial u}{\partial x}\frac{\partial^2 u}{\partial y^2}-\frac{\partial u}{\partial y}\frac{\partial^2 v}{\partial y^2}\right] \\ &+g\,\beta_T\,(T-T_\infty)\,\mathrm{Sin}\frac{\alpha}{2}, \end{aligned} \tag{2}$$

$$\rho c_p\left(u\frac{\partial T}{\partial x}+v\frac{\partial T}{\partial y}\right)=\frac{\partial}{\partial y}\left(\left(\frac{16\sigma^* T_\infty^3}{3k^*}+k_T\right)\frac{\partial T}{\partial y}\right). \tag{3}$$

The appropriate boundary conditions are

$$\begin{aligned} &u=U, \quad v=0, \quad T=T_w=T_\infty+Ax^k \\ &\quad \text{at } y=0, \\ &u\to 0, \quad T\to T_\infty \quad \text{as } y\to\infty \end{aligned} \tag{4}$$

where $U\left(=ax^n\right)$ is the free stream velocity, μ is the dynamic viscosity, λ_1 is the relaxation time, λ_2

is the retardation time, α is the wedge angle, k_T is the thermal conductivity, k is the surface temperature exponent, T and T_∞ are the temperatures of the fluid and ambient respectively and T_w is the wall temperature. We utilize **[13 20, 21]**

$$u = U(x) f', \quad \eta = \sqrt{\frac{n+1}{2}} \sqrt{\frac{U}{\nu x}} y,$$

$$\psi = \sqrt{\frac{2}{n+1}} \sqrt{\nu x U} f(\eta), \tag{5}$$

$$v = -\sqrt{\frac{n+1}{2}} \sqrt{\frac{\nu U}{x}} \left[f(\eta) + \frac{n-1}{n+1} \eta f'(\eta) \right], \quad \theta(\eta) = \frac{T - T_\infty}{T_w - T_\infty}, \tag{6}$$

where η is the similarity variable, ψ is the stream function, f is the dimensionless stream function and θ is the dimensionless temperature. Now the continuity equation (1) is identically satisfied and Eqs. $(2)-(4)$ leads

$$f''' + ff'' + \beta_1 \begin{pmatrix} -2n\left(\frac{n-1}{n+1}\right) f'^3 \\ +(3n-1) f f' f'' \\ -\left(\frac{n+1}{2}\right) f^2 f''' + \\ \left(\frac{n-1}{2}\right) \eta f'^2 f'' \end{pmatrix} + \beta_2 \begin{pmatrix} \left(\frac{3n-1}{2}\right) (f'')^2 - \\ \left(\frac{n+1}{2}\right) f f'''' + \\ (n-1) f f''' \end{pmatrix} - \frac{2n}{n+1} f'^2 + \frac{2}{n+1} \lambda \theta \sin\frac{\alpha}{2} = 0, \tag{7}$$

$$\left(1 + \frac{4}{3} R\right) \theta'' + \Pr\left(f \theta' - \frac{2k}{n+1} f' \theta\right) = 0, \tag{8}$$

$$f(0) = 0,\ f'(0) = 1, \quad \theta(0) = 1, \quad f'(\infty) = 0, \quad \theta(\infty) = 0, \tag{9}$$

Here prime denotes the differentiation with respect to η, β_1 and β_2 are the dimensionless material parameters, λ is mixed convection parameter, Gr_x is the local Grashof number, $\Pr$ is the Prandtl number and R is the radiation parameter. The definitions of these parameters are

$$\beta_1 = \frac{\lambda_1 U}{x}, \beta_2 = \frac{\lambda_2 U}{x}, \lambda = \frac{Gr_x}{\mathrm{Re}_x^2}, \Pr = \frac{\mu c_p}{k}, \quad R = \left(\frac{4\sigma^* T_\infty^3}{k^* k}\right), Gr_x = \frac{g\beta(T_w - T_\infty)x^3}{\upsilon^2}. \tag{10}$$

Local Nusselt number (Nu_x) along with heat transfer rate (q_w) are

$$Nu_x = \frac{x q_w}{k(T_w - T_\infty)}, \quad q_w = -k\left(\frac{\partial T}{\partial y}\right)_{y=0} \tag{11}$$

which in dimensionless form gives

$$(\mathrm{Re}_x)^{-1/2} Nu_x = -\theta'(0). \tag{12}$$

Series solutions

The initial guesses (f_0, θ_0) and auxiliary linear operators (L_f, L_θ) are taken as follows

$$f_0(\eta) = 1 - e^{-\eta}, \qquad \theta_0(\eta) = e^{-\eta}, \tag{13}$$

$$\mathbf{L}_f(f) = \frac{d^3 f}{d\eta^3} - \frac{df}{d\eta}, \quad \mathbf{L}_\theta(\theta) = \frac{d^2\theta}{d\eta^2} - \theta, \tag{14}$$

With

$$\mathbf{L}_f\left[C_1 + C_2 \exp(\eta) + C_3 \exp(-\eta)\right] = 0, \tag{15}$$

$$\mathbf{L}_\theta\left[C_4 \exp(\eta) + C_5 \exp(-\eta)\right] = 0, \tag{16}$$

where C_i $(i = 1-5)$ are the arbitrary constants. If $p \in [0,1]$ is the embedding parameter and $\hbar_f$ and $\hbar_\theta$ are the non-zero auxiliary parameters then the zeroth-order and m th order deformation problems are stated as follows.

Zeroth order problem

$$(1-p)\mathbf{L}_f\begin{bmatrix} \hat{f}(\eta;p) \\ -f_0(\eta) \end{bmatrix} = p\hbar_f \mathbf{N}_f\left[\hat{f}(\eta;p), \hat{\theta}(\eta;p)\right], \tag{17}$$

$$(1-p)\mathbf{L}_\theta\begin{bmatrix} \hat{\theta}(\eta;p) \\ -\theta_0(\eta) \end{bmatrix} = p\hbar_\theta \mathbf{N}_\theta\left[\hat{\theta}(\eta;p), \hat{f}(\eta;p)\right], \tag{18}$$

$$\hat{f}(0;p) = 0,\ \hat{f}'(0;p) = 0,\ \hat{f}'(\infty;p) = 1, \tag{19}$$

$$\hat{\theta}(0;q) = 1, \quad \hat{\theta}(\infty;q) = 0, \tag{20}$$

$$\begin{aligned} \mathbf{N}_f\left[\hat{f}(\eta,p), \hat{\theta}(\eta;p)\right] = {} & \frac{\partial^3 f(\eta;p)}{\partial\eta^3} \\ & + f(\eta;p)\frac{\partial^2 f(\eta;p)}{\partial\eta^2} \\ & - \frac{2n}{n+1}\left(\frac{\partial f(\eta;p)}{\partial\eta}\right)^2 \\ & + \beta_1 \begin{pmatrix} -2n\,\frac{n-1}{n+1}\left(\frac{\partial f(\eta;p)}{\partial\eta}\right)^3 \\ +(3n-1) f(\eta;p) \\ \frac{\partial f(\eta;p)}{\partial\eta}\frac{\partial^2 f(\eta;p)}{\partial\eta^2} \\ -\frac{n+1}{2}\left(f(\eta;p)\right)^2 \frac{\partial^3 f(\eta;p)}{\partial\eta 3} \\ +\frac{n-1}{2}\eta\left(\frac{\partial f(\eta;p)}{\partial\eta}\right)^2 \frac{\partial^2 f(\eta;p)}{\partial\eta^2} \end{pmatrix} \end{aligned}$$

$$+\beta_2\begin{pmatrix} \left(\frac{3n-1}{2}\right)\left(\frac{\partial^2 f(\eta;p)}{\partial\eta^2}\right)^2 \\ -\left(\frac{n+1}{2}\right)f(\eta;p)\frac{\partial^4 f(\eta;p)}{\partial\eta^4} \\ +(n-1)\frac{\partial f(\eta;p)}{\partial\eta}\frac{\partial^3 f(\eta;p)}{\partial\eta^3} \end{pmatrix} + \frac{2}{n+1}\lambda\hat{\theta}(\eta,p)\sin\frac{\alpha}{2}, \tag{21}$$

$$\mathbf{N}_\theta\left[\hat{\theta}(\eta;p),\hat{f}(\eta;p)\right] = \left(1+\frac{4}{3}R\right)\frac{\partial^2\hat{\theta}(\eta,p)}{\partial\eta^2} + \Pr\begin{pmatrix} \hat{f}(\eta;p)\frac{\partial\hat{\theta}(\eta;p)}{\partial\eta} \\ -\frac{2k}{n+1}\hat{\theta}(\eta;p)\frac{\partial\hat{f}(\eta;p)}{\partial\eta} \end{pmatrix}. \tag{22}$$

m th-order deformation problems

$$\mathbf{L}_f\left[f_m(\eta)-\chi_m f_{m-1}(\eta)\right] = \hbar_f\,\mathbf{R}_m^f(\eta), \tag{23}$$

$$\mathbf{L}_\theta\left[\theta_m(\eta)-\chi_m\theta_{m-1}(\eta)\right] = \hbar_\theta\mathbf{R}_m^\theta(\eta), \tag{24}$$

$$f_m(0)=f_m'(0)=f_m'(\infty)=f_m''(\infty)=0, \tag{25}$$

$$\theta_m(0)=\theta_m(\infty)=0, \tag{26}$$

$$\mathbf{R}_m^f(\eta) = f_{m-1}'''(\eta) + \sum_{k=0}^{m-1}\begin{bmatrix} f_{m-1-k}f_k'' - \frac{2n}{n+1}f_{m-1-k}'f_k' \\ +\beta_1\begin{pmatrix} -2n\frac{n-1}{n+1}f_{m-1-k}'\sum_{l=0}^{k}f_{k-l}'f_l' \\ +(3n-1)f_{m-1-k}\sum_{l=0}^{k}f_{k-l}'f_l'' \\ -\frac{n+1}{2}f_{m-1-k}\sum_{l=0}^{k}f_{k-l}f_l''' \\ +\frac{n-1}{2}\eta f_{m-1-k}'\sum_{l=0}^{k}f_{k-l}'f_l'' \end{pmatrix} \\ +\beta_2\begin{pmatrix} \frac{3n-1}{2}f_{m-1-k}''f_k'' \\ -\frac{n+1}{2}f_{m-1-k}f_k'''' \\ +(n-1)f_{m-1-k}'f_k''' \end{pmatrix} \end{bmatrix} + \frac{2}{n+1}\lambda\theta_{m-1}\sin\frac{\alpha}{2}, \tag{27}$$

$$\mathbf{R}_m^\theta(\eta) = \theta_{m-1}'' + \Pr\sum_{k=0}^{m-1}\left(\theta_{m-1-k}'f_k - \frac{2k}{n+1}f_{m-1-k}'\theta_k\right), \tag{28}$$

$$\chi_m = \begin{cases} 0, & m\le 1 \\ 1, & m>1 \end{cases}. \tag{29}$$

For $p=0$ and $p=1$, we have

$$\hat{f}(\eta;0)=f_0(\eta),\hat{f}(\eta;1)=f(\eta), \tag{30}$$

$$\hat{\theta}(\eta;0)=\theta_0(\eta),\ \hat{\theta}(\eta;1)=\theta(\eta), \tag{31}$$

and when p increases from 0 to 1 then $\hat{f}(\eta;p)$ and $\hat{\theta}(\eta;p)$ vary from the initial solutions $f_0(\eta)$ and $\theta_0(\eta)$ to final solutions $f(\eta)$ and $\theta(\eta)$ respectively. By Taylor's expansion one has

$$\hat{f}(\eta;p)=f_0(\eta)+\sum_{m=1}^{\infty}f_m(\eta)p^m, \quad f_m(\eta)=\frac{1}{m!}\left.\frac{\partial^m\hat{f}(\eta;p)}{\partial p^m}\right|_{p=0}, \tag{32}$$

$$\hat{\theta}(\eta;p)=\theta_0(\eta)+\sum_{m=1}^{\infty}\theta_m(\eta)p^m, \quad \theta_m(\eta)=\frac{1}{m!}\left.\frac{\partial^m\hat{\theta}(\eta;p)}{\partial p^m}\right|_{p=0}, \tag{33}$$

where the auxiliary parameters are so properly chosen that the series (32) and (33) converge at $p=1$ i.e.

$$f(\eta)=f_0(\eta)+\sum_{m=1}^{\infty}f_m(\eta), \tag{34}$$

$$\theta(\eta)=\theta_0(\eta)+\sum_{m=1}^{\infty}\theta_m(\eta). \tag{35}$$

The general solutions are

$$f_m(\eta)=f_m^*(\eta)+C_1+C_2e^{\eta}+C_3e^{-\eta}, \tag{36}$$

$$\theta_m(\eta)=\theta_m^*(\eta)+C_4e^{\eta}+C_5e^{-\eta}, \tag{37}$$

In which f_m^* and $\theta_m^*(\eta)$ are special functions.

Convergence of the series solutions

Note that the series solutions in Eqs. (34) and (35) contain two auxiliary parameters $\hbar_f$ and $\hbar_\theta$. The convergence of series solutions depend upon these auxiliary parameters. For range of values of these parameters, the $\hbar-$ curves at 15 th-order of approximations have been plotted in Fig. 2. It is found that the admissible values of $\hbar_f$ and $\hbar_\theta$ are $-1.3\le\hbar_f\le-0.25$ and $-1.2\le\hbar_\theta\le-0.5$. The series converge in the whole region of η when $\hbar_f=\hbar_\theta=-1.0$. The residual errors of f and θ are

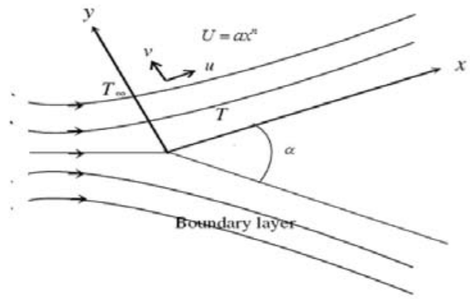

Fig. 1. Physical Model.

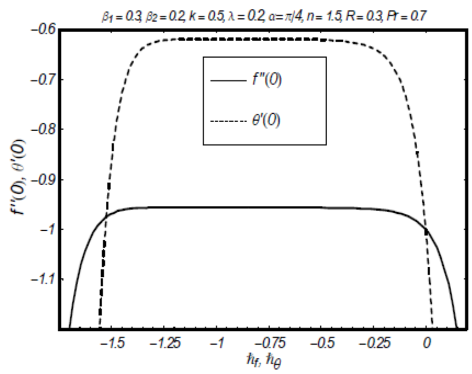

Fig. 2. $\hbar$ -curves for the functions f and θ.

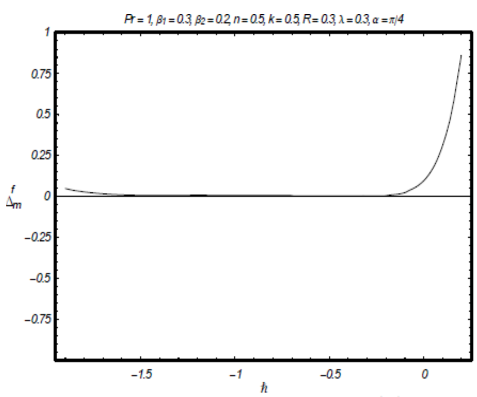

Fig. 2a. Residual Error for $f(\eta)$.

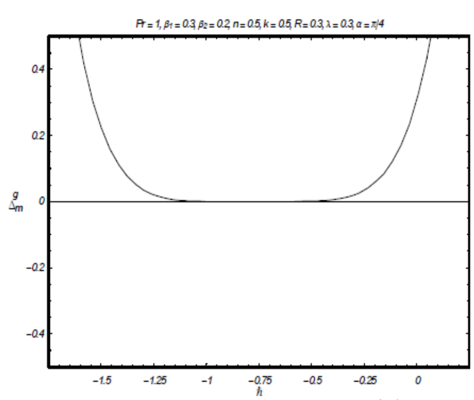

Fig. 2b. Residual Error for $g(\eta)$.

Residual error of

$$f = f_m''' + f_m f_m'' + \beta_1\left(-2n\left(\frac{n-1}{n+1}\right) f_m'^3 + (3n-1) f_m f_m' f_m'' - \left(\frac{n+1}{2}\right) f_m^2 f_m''' + \left(\frac{n-1}{2}\right)\eta f_m'^2 f_m''\right)$$
$$+\beta_2\left(\left(\frac{3n-1}{2}\right)\left(f_m''\right)^2 - \left(\frac{n+1}{2}\right) f_m f_m'''' + (n-1) f_m' f_m'''\right) - \frac{2n}{n+1} f_m'^2 + \frac{2}{n+1}\lambda\theta_m \sin\frac{\alpha}{2},$$

Residual error of

$$\theta = \left(1+\frac{4}{3}R\right)\theta_m'' + \Pr\left(f_m\theta_m' - \frac{2k}{n+1} f_m'\theta_m\right) = 0,$$

3. DISCUSSION

The aim of this subsection is to present the effects of pertinent parameters on the velocity, temperature and surface heat transfer. Figs. 3 and 4 are displayed to see the effects of β_1 on the velocity and temperature profiles. It is observed that both the velocity profile and momentum boundary layer thickness decrease by increasing β_1. However the thermal boundary layer thickness and temperature increase. The dependence of material parameter β_2 on the velocity and temperature profiles are shown in the Figs. 5 and 6 respectively. These Figs. indicate that the velocity profile and momentum boundary layer thickness are increasing functions of β_2 while reverse behavior is observed in the case of temperature and thermal boundary layer thickness.

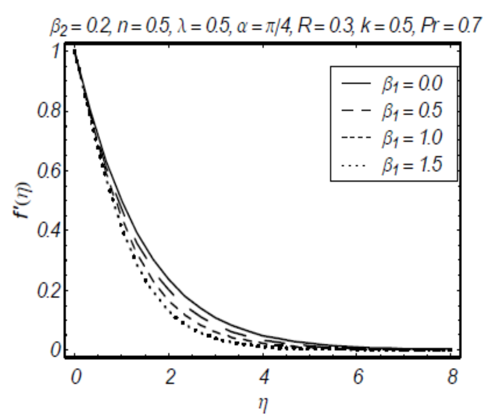

Fig. 3. Influence of β_1 on $f'(\eta)$.

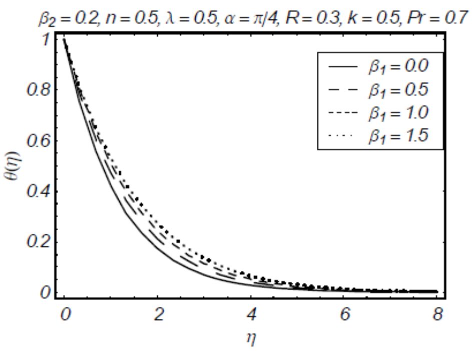

Fig. 4. Influence of β_1 on $\theta(\eta)$.

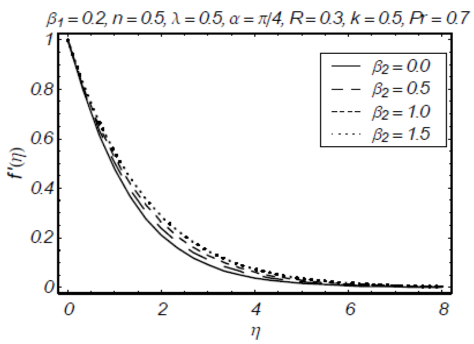

Fig. 5. Influence of β_2 on $f^{/}(\eta)$.

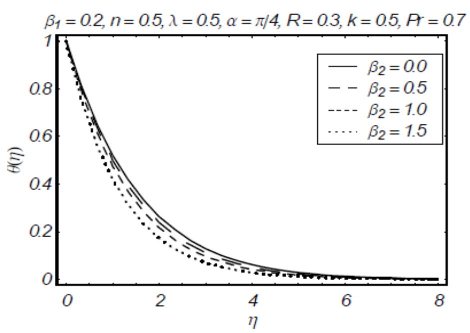

Fig. 6. Influence of β_2 on $\theta(\eta)$.

Variation of parameter n on the velocity and temperature are sketched in the Figs. 7 and 8. Clearly the effects of n on the velocity and temperature profiles are quite reverse. Influence of mixed convection parameter λ on both the velocity and temperature profiles are given in the Figs. 9 and 10. It is observed that the velocity and momentum boundary layer thickness increase with the increase of mixed convection parameter λ while the temperature and thermal boundary layer thickness decrease. Figs. 11 and 12 are drawn to see the variation of α on the velocity and temperature profiles. It is noticed that the velocity and momentum boundary layer thickness increase when α increases It is also found that the temperature and thermal boundary layer thickness are increasing functions of α. We have drawn Figs. 13 and 14 to see the variation of radiation parameter R on the velocity $f'(\eta)$ and temperature $\theta(\eta)$ profiles.

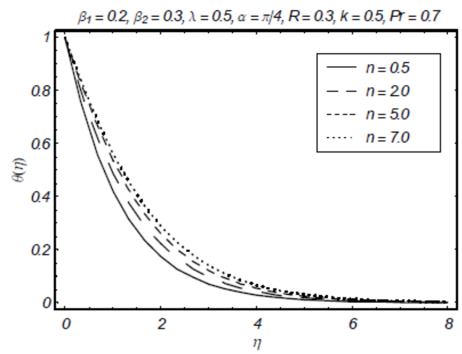

Fig. 8. Influence of n on $\theta(\eta)$.

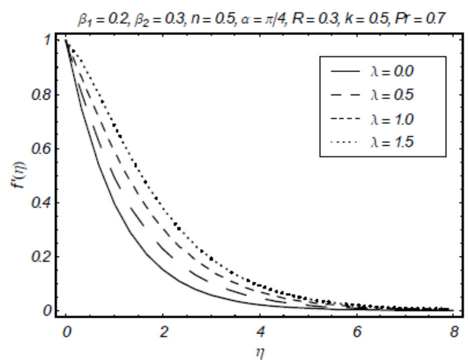

Fig. 9. Influence of λ on $f^{/}(\eta)$.

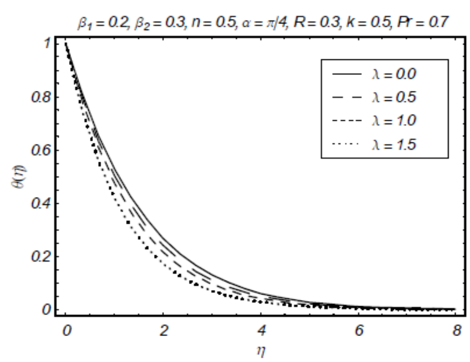

Fig. 10. Influence of λ on $\theta(\eta)$.

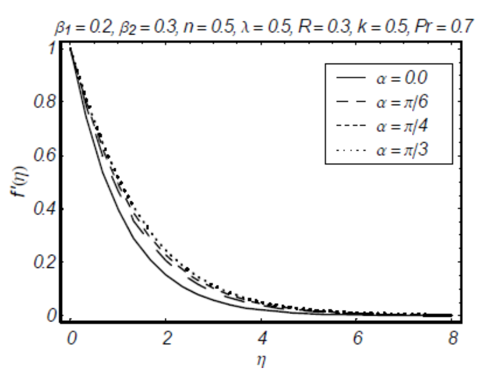

Fig. 11. Influence of α on $f^{/}(\eta)$.

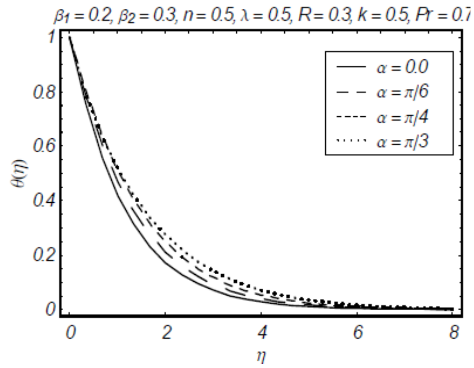

Fig. 12. Influence of α **on** $\theta(\eta)$.

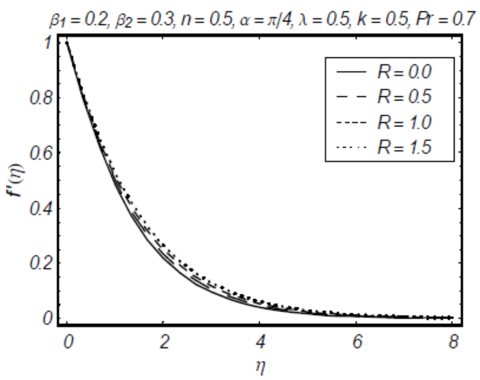

Fig. 13. Influence of R **on** $f^{\prime}(\eta)$.

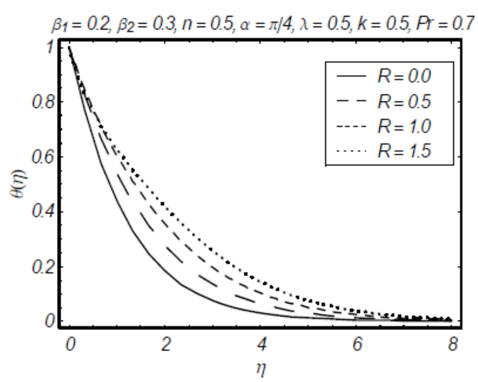

Fig. 14. Influence of R **on** $\theta(\eta)$.

It is seen that the effect of R on both the temperature and velocity profiles are similar. It is further noted that the momentum and thermal boundary layer thicknesses are increasing functions of R. Figs. 15 and 16 are sketched to see the variation of surface temperature parameter k on the velocity $f'(\eta)$ and the temperature $\theta(\eta)$. Both $f'(\eta)$ and $\theta(\eta)$ decrease with the increase in k. It is also observed that both the momentum and thermal boundary layer thicknesses decrease when k increases. Influence of Prandtl number Pr on the velocity and temperature profiles are shown in the Figs. 17 and 18. These Figs. show that by increasing the values of Pr both the velocity and temperature profiles decrease.

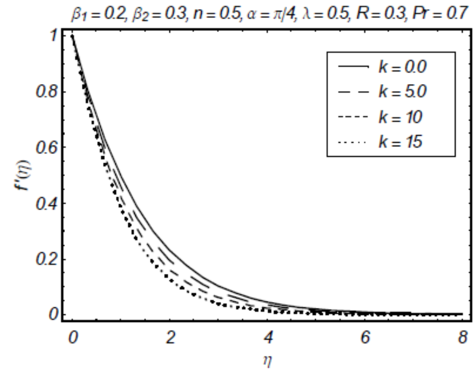

Fig. 15. Influence of k **on** $f^{\prime}(\eta)$.

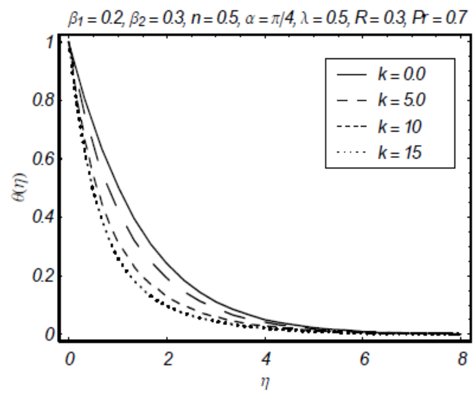

Fig. 16. Influence of k **on** $\theta(\eta)$.

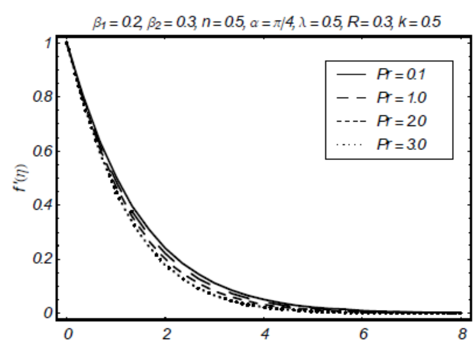

Fig. 17. Influence of Pr **on** $f^{\prime}(\eta)$.

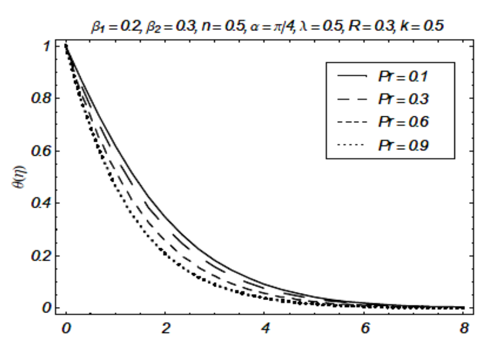

Fig. 18. Influence of Pr **on** $\theta(\eta)$.

The momentum and thermal boundary layer thicknesses also decrease by increasing Pr. Clearly an increase in the values of Pr leads to a decrease in the thermal diffusivity. Figs. 19 – 22 are drawn to see the influence of Deborah numbers β_1 and β_2, mixed convection parameter λ, wedge angle α, radiation parameter R, Prandtl number Pr, surface temperature parameter k and velocity index n on the local Nusselt number $-\theta'(0)$. It is observed from Fig. 19 that β_1 and β_2 have quite opposite effects near the wall on the local Nusselt number $-\theta'(0)$ i.e an increase in β_1 leads to decrease in local Nusselt number $-\theta'(0)$. Away from the wall, $-\theta'(0)$ decreases for increasing values of β_2. Fig. 20 depicts the effects of λ and α on $-\theta'(0)$. It is noticed that $-\theta'(0)$ increases through increase of mixed convection parameter λ and wedge angle α. Fig. 21 depicts that variation of n and k have opposite effects on $-\theta'(0)$. It is noted that $-\theta'(0)$ is decreasing function of R while increasing function of Pr (see Fig. 22). A close look at Table 1 indicates that 25[th] -order approximation gives convergent series solutions.

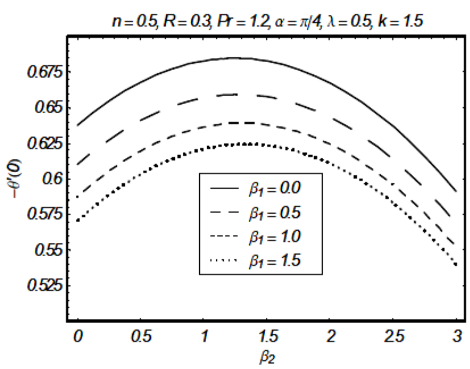

Fig. 19. Influence of β_1 and β_2 on $\theta'(0)$.

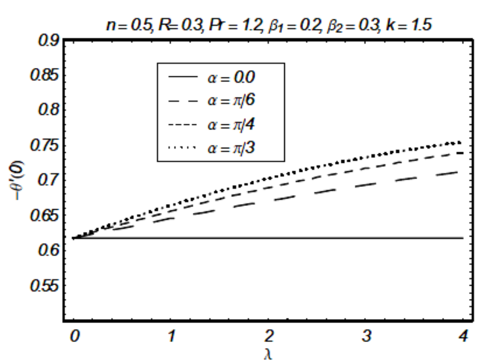

Fig. 20. Influence of λ and α on $\theta'(0)$.

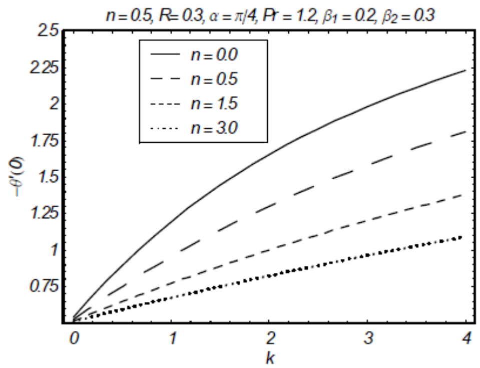

Fig. 21. Influence of n and k on $\theta'(0)$.

Table 1 Convergence of the homotopy solutions for different order of approximation when $\Pr = 1.0$, $\lambda = 0.3$, $n = 1.5$, $k = 0.5$, **R = 0.3, k = 0.5,** $\alpha = \pi/4$, $\beta_1 = 0.2$, $\beta_2 = 0.3$ **and** $\hbar_f = \hbar_\theta = -0.5$

Order of approximation	$-f''(0)$	$-\theta'(0)$
1	0.90330	0.78889
5	0.86304	0.64042
10	0.86077	0.62757
15	0.86047	0.62627
20	0.86045	0.62616
25	0.86044	0.62616
30	0.86044	0.62616

4. CONCLUSIONS

Mixed convection effects in the Falkner-Skan wedge flow of an Oldroyd-B fluid are investigated. Analysis is modeled and analyzed in the presence of thermal radiation. The following points are worth mentioning:

Table 1 shows that convergence of the functions f and θ are obtained at 25[th] -order approximations up to five decimal places when $\hbar_f = \hbar_\theta = -0.5$.

Thermal boundary layer thickness increases with the material parameter β_1 while reverse behavior is seen in case of momentum boundary layer thickness.

Influence of mixed convection parameter λ increases the velocity and momentum boundary layer thickness while it decreases the temperature and thermal boundary layer thickness.

An increase in material parameter β_2 increases the velocity and reduces the thermal boundary layer thickness.

Both temperature and thermal boundary layer thickness decrease when the Prandtl number Pr is increased.

Influence of wedge angle α and radiation parameter R on both the temperature and velocity profiles are quite similar.

Thermal boundary layer and momentum boundary layer thicknesses are decreasing functions of surface temperature exponent k .

Surface heat transfer $-\theta'(0)$ increases with an increase of wedge angle α, mixed convection parameter λ, radiation parameter R, Prandtl number Pr and surface temperature exponent k .

In case of material parameter β_1 the surface heat transfer $-\theta'(0)$ decreases while the material parameter β_2 decreases it near the boundary and increases far away.

ACKNOWLEDGMENT

The research work of Dr. Alsulami was partially supported by the Deanship of Scientific Research (DSR), King Abdulaziz University, Jeddah, Saudi Arabia.

REFRENCES

Abbasbandy, S. and T. Hayat (2009). Solution of the MHD Falkner-Skan flow by Hankel-Pad´e method. *Physics Letters A 373,731-734*.

Abbasbandy, S. and T. Hayat (2009). Solution of the MHD Falkner-Skan flow by homotopy analysis method. *Communications in Nonlinear Science and Numerical Simulation14, 3591-3598.*

Abbasbandy, S., M. S. Hashemi and I. Hashim (2013). On convergence of homotopy analysis method and its application to fractional integro-differential equations. *Quaestiones Mathematicae 3 93-105.*

Ashraf, M. B., T. Hayat and A. Alsaedi (2015). Three-dimensional flow of Eyring-Powell nanofluid by convectively heated exponentially stretching sheet. *The European Physical Journal Plus 130:5*

Chen, C. H. (2009). Magneto-hydrodynamic mixed convection of a power-law fluid past a stretching surface in the presence of thermal radiation and internal heat generation/absorption. *International Journal of Non-Linear Mechanics 44, 596-603.*

Falkner V. M. and S. W. Skan (1931). Some approximate solutions of the boundary layer equations. *Philosophical Magazine* 12 (1931) 865-896.

Fetecau, C., C. Fetecau, M. Kamran and D. Vieru (2009). Exact solutions for the flow of a generalized Oldroyd-B fluid induced by a constantly accelerating plate between two side walls perpendicular to the plate. *Journal of Non-Newtonian Fluid Mechanics* **156** *(3), 189-201.*

Fetecau, C., J. Zierep, R. Bohning and C. Fetecau (2010). On the energetic balance for the flow of an Oldroyd-B fluid due to a flat plate subject to a time-dependent shear stress. *Computers & Mathematics with Applications 60(1), 74-82.*

Fetecau, C., T. Hayat, J. Zierep and M. Sajid. Energetic balance for the Rayleigh--Stokes problem of an Oldroyd-B fluid. *Nonlinear Analysis: Real World Appl. 12(2011), 1-13.*

Haitao, Q. and H. Jin (2009). Unsteady helical flows of a generalized Oldroyd-B fluid with fractional derivative. *Nonlinear Analysis: Real World Applications* **10** *(5), 2700-2708.*

Haitao, Q. and X. Mingyu (2009). Some unsteady unidirectional flows of a generalized Oldroyd-B fluid with fractional derivative. *Applied Mathematical Modelling* **33** *(11), 4181-4191*.

Hartree, D. R. (1937). On equations occurring in Falkner and Skan's approximate treatment of the equations of boundary layer. *Proceedings* of the *Cambridge Philosophical Society* 33, 223-239.

Hayat, T. , M. Hussain, S. Nadeem and S. Mesloub (2011). Falkner-Skan wedge flow of a power-law fluid with mixed convection and porous medium. *Computers & Fluids 49, 22-28.*

Hayat, T , M. Qasim and Z. Abbas (2010). Radiation and mass transfer effects on the magnetohydrodynamic unsteady flow induced by a stretching sheet. *Zeitschrift für Naturforschung A 65, 231-239.*

Hayat, T., S. A. Shehzad, M. B. Ashraf and A. Alsaedi (2013). Magnetohydrodynamic mixed convection flow of thixotropic fluid with thermophoresis and Joule heating. *Journal of Thermophysics and Heat Transfer 27, 733-740.*

Hayat, T., S. A. Shehzad, M. Mustafa and A. Hendi (2012). MHD flow of an Oldroyd-B fluid through a porous channel. *International Journal of Chemical Reactor Engineering 10 (1), A8.*

Ishak, A. (2010). Similarity solutions for flow and heat transfer over a permeable surface with convective boundary condition. *Applied Mathematics and Computation 217, 837-842.*

Jamil, M., N. A. Khan and A. A. Zafar (2011). Translational flows of an Oldroyd-B fluid with fractional derivatives. *Computers & Mathematics with Applications 62(3), 1540-1553.*

Kim, Y. J. (2001). The Falkner- Skan wedge flows of power-law fluids embedded in a porous medium. *Transport in Porous Media 44, 267-279.*

Kuo, B. L. (2005). Heat transfer analysis for the Falkner-Skan wedge flow by the differential transformation method. *International Journal of Heat and Mass Transfer 48(2005), 5036-5046.*

Liao, S. (2012). *Homotopy analysis method in nonlinear differential equations*. Higher Edu. Press, Beijing and Springer-Verlag Berlin Heidelberg.

Liu, Y., L. Zheng and X. Zhang (2011). Unsteady MHD Couette flow of a generalized Oldroyd-B fluid with fractional derivative. *Computers 8 Mathematics with Applications 61(2), 443-450.*

Liu, Y. P., S. J. Liao and Z. B. Li (2013). Symbolic computation of strongly nonlinear periodic oscillations. *Journal of Symbolic Computation 55, 72-95.*

Mukhopadhyay, S. (2009). Effects of radiation and variable fluid viscosity on flow and heat transfer along a symmetric wedge. *Journal of Applied Fluid Mechanics 2, 29-34.*

Prand, K., A. R. Razaei and S. M. Ghaderic (2010). An approximate solution to the MHD Falkner-Skan flow by Hermite functions pseudospectral method. *Communications in Nonlinear Science and Numerical 16, 274-283.*

Rashidi, M. M., N. kavyani and S. Abelman (2014). Investigation of entropy generation in MHD and slip flow over a rotating porous disk with variable properties. *International Journal of Heat and Mass Transfer 70, 892-917.*

Turkyilmazoglu, M. (2012). Solution of Thomas-Fermi equation with a convergent approach. *Communications in Nonlinear Science and Numerical Simulation 17, 4097-4103.*

Zheng, L., Z. Guo and X. Zhang (2011). 3D flow of a generalized Oldroyd-B fluid induced by a constant pressure gradient between two side walls perpendicular to a plate. *Nonlinear Analysis: Real World Applications 12(6), 3499-3508.*

Zheng, L., J. Niu, X. Zhang and Y. Gao (2012). MHD flow and heat transfer over a porous shrinking surface with velocity slip and temperature jump. *Mathematical and Computer Modelling 56, 133-144.*

Zheng, L., Y. Liu and X. Zhang (2011). Exact solutions for MHD flow of generalized Oldroyd-B fluid due to an infinite accelerating plate. *Mathematical and Computer Modelling 54(1-2), 780-788.*